Fuel 297 (2021) 120758

Contents lists available at ScienceDirect

Fuel

journal homepage: www.elsevier.com/locate/fuel

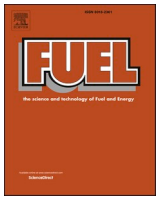

Full Length Article

The effects of particle size on flameless combustion characteristics and NO_x emissions of semi-coke with coal preheating technology

Hongliang Ding [a,b], Ziqu Ouyang [a,b,*], Xiaoyu Zhang [a,c], Shujun Zhu [a,d]

[a] Institute of Engineering Thermophysics, Chinese Academy of Sciences, Beijing 100190, China
[b] University of Chinese Academy of Sciences, Beijing 100049, China
[c] University of Science and Technology of China, Hefei 230026, China
[d] State Key Laboratory of High-temperature Gas Dynamics, Institute of Mechanics, Chinese Academy of Sciences, Beijing 100190, China

ARTICLE INFO

Keywords:
Particle size
Self-preheating
Flameless combustion
NO_x emissions

ABSTRACT

The experiments of the effect of particle size on flameless combustion characteristics and NO_x emissions of Shenmu semi-coke were launched on a bench-scale coal preheating combustion test rig. The results revealed that the difference of fuel particle size greatly influenced the yield of each component in high-temperature coal gas and the reactive activity of coal char, thus subsequently affecting the final combustion process and NO_x emissions. The specific surface area and pore volume of Shenmu semi-coke were both significantly increased after preheated, leading to a better reactivity and the improved combustion performance, especially when d_{50} (the mean particle size) = 163.84 μm, where the temperature of the down-fired combustor reached the highest. The different particle size of Shenmu semi-coke resulted in different preheating temperature, which further affected the content of each component in the high-temperature coal gas. During the self-preheating process, most volatile matter and fuel bound N were separated out and the released N was mainly converted to N_2 and NH_3, besides the conversion rate of each component (C, H, N and V) was the highest when d_{50} = 100.17 μm. Additionally, all experimental conditions achieved flameless combustion, with a transparent combustion area, but no flame front visible to the naked eye, and the highest combustion efficiency was 98.23% when d_{50} = 163.84 μm with the brightest flame image. It was discovered in this experimental that there was a critical value (d_{50} = 198.54 μm) of Shenmu semi-coke particles. When the particle size was lower than or higher than the critical value, NO_x generated by combustion would decrease. The lowest NO_x emission was 89.46 mg/m^3 (@6% O_2) when d_{50} was 35.34 μm.

1. Introduction

Coal, collectively known as three pillar energy sources with oil and natural gas in today's world economy, has played a prominent role in pushing forward the operation and development of the entire world economy for a long time [1–3]. In China, the gradient utilization has been one of the important ways for the clean and efficient use of coal in the burgeoning coal chemical industry. The power generation by burning low-volatile fuel such as coal gasification fly ash (CGFA) [4,5] and semi-coke (by-products of coal pyrolysis) [6,7] as high-grade clean fuel is an important component to realize the clean and efficient gradient utilization of coal. Due to the large energy demand and long time for combustion of low-volatile fuel, the stability of combustion must be taken into consideration [8–12]. By virtue of the large number of regenerative bed materials, the combustion stability of circulating fluidized bed (CFB) is excellent and low-volatile fuel can be available for combustion. Ren [13] realized the stable combustion of ultra-fine gasified carbon residue (V_{daf} < 2%) on a pilot CFB test stand, with NO_x emissions ranging from 200 mg/m^3 to 300 mg/m^3 (@6% O_2). And the calculated combustion efficiency (η) can be up to 98%. In the literature [14–16], controlling the amount of air in CFB and adding air to the outlet of cyclone separator for supplementary after-burning can also effectively reduce NO_x emissions during the combustion of low-volatile fuel. The operation results reveal that stable combustion of Shenmu semi-coke can be realized, moreover, NO_x emissions were controlled within 100 mg/m^3 (@6% O_2).

To solve the problems in the combustion process of low-volatile fuel and meet the strict environmental protection requirements, great efforts

* Corresponding author at: Institute of Engineering Thermophysics, Chinese Academy of Sciences, 11Beisihuanxi Road, Haidian District, Beijing 100190, China.
E-mail address: ouyangziqu@iet.cn (Z. Ouyang).

https://doi.org/10.1016/j.fuel.2021.120758
Received 20 December 2020; Received in revised form 22 March 2021; Accepted 24 March 2021
Available online 5 April 2021

should be made to find out the effective combustion technology for de-NO_x. Flameless combustion [17–23] is a new sort of combustion technology that sprung up in the past three decades, featuring uniform temperature distribution in the combustion zone, low peak temperature, high combustion efficiency (η), and low-NO_x emissions, besides no apparent flame front occurs in the combustion process. Due to its potential on NO_x reduction, an increasing number of researchers started to pay close attention to flameless combustion technology, which is known as the most promising combustion technology in the 21st century [20,22].

With the original creativity, coal self-preheating combustion technology proposed by the institute of Engineering Thermophysics, Chinese Academy of Sciences, is also a highly efficient and clean combustion technology that has been applied in many projects [24]. The high-temperature coal gas and coal char produced by a self-preheating burner have good combustion characteristics, which makes fuel stripped of nitrogen early. Combined with coal self-preheating combustion technology that owns distinct characteristic and evident advantage, the stable and high effective combustion and low/ultra-low NO_x emissions of various fuels can be easier achieved. Previous researches have proved its potential on NO_x reduction for anthracite, semi-coke and coal gasification fly ash in a bench-scale apparatus [25–28] and a pilot-scale apparatus [29,30].

The combustion characteristics of pulverized coal are closely related to coal quality, reaction atmosphere and particle size. Among them, particle size is the most basic and important parameter in the physical structure of pulverized coal. Due to the difference of fuel particle size, the reactivity of fuel itself, the residence time in the reactor, and the combustion temperature will all be different, which greatly influences the final combustion process and NO_x emissions [31–33]. In this study, six kinds of Shenmu semi-coke (quenching after the pyrolysis of Shenmu bituminous coal) with different particle size were used as fuel to conduct relevant exploratory experiments. Under the conditions of Shenmu semi-coke with different particle size, the behavior characteristics of combustion in the entire process and pollutant formation regularity were discussed.

2. Experimental

2.1. Test rig

A 30 kW pulverized coal flameless combustion experiment rig was designed, composed of a self-preheating burner, a down-fired combustor (DFC) and other auxiliary systems. The Schematic diagram of the self-preheating burner and the DFC are both shown in Fig. 1.

The self-preheating burner was designed based on a CFB prototype, made of heat resistant steel, and composed of a riser, a cyclone separator, a loop seal recovery device and other components. The primary air was supplied from the bottom of the riser which had an inner diameter of 90 mm and a height of 1500 mm, with a volume about 20%-40% of the theoretical air volume. The fuel entered the self-preheating burner quickly ignited and partially burned under the action of high-temperature bed material, heating itself to above 800 °C. After pulverized coal passed through the self-preheating burner, high-temperature coal gas and coal char (collectively referred to as preheated fuel) were generated and subsequently entered the DFC from the cyclone separator.

The DFC had an inner diameter of 300 mm and a height of 3500 mm, with a preheated fuel nozzle and a secondary air nozzle set on the top. A multi-channel coaxial jet nozzle as shown in Fig. 2 was used in this experiment. Discharged from the center cylinder of the cyclone separator, the preheated fuel was then injected into the DFC. The inner and outer secondary air channel were respectively set on the middle layer and the outermost layer. Additionally, there were three layers of tertiary air nozzles at the position of 500 mm, 1000 mm and 1500 mm below the top of the DFC with separate valve and flow meter on each layer, which could be controlled according to the experimental conditions. The

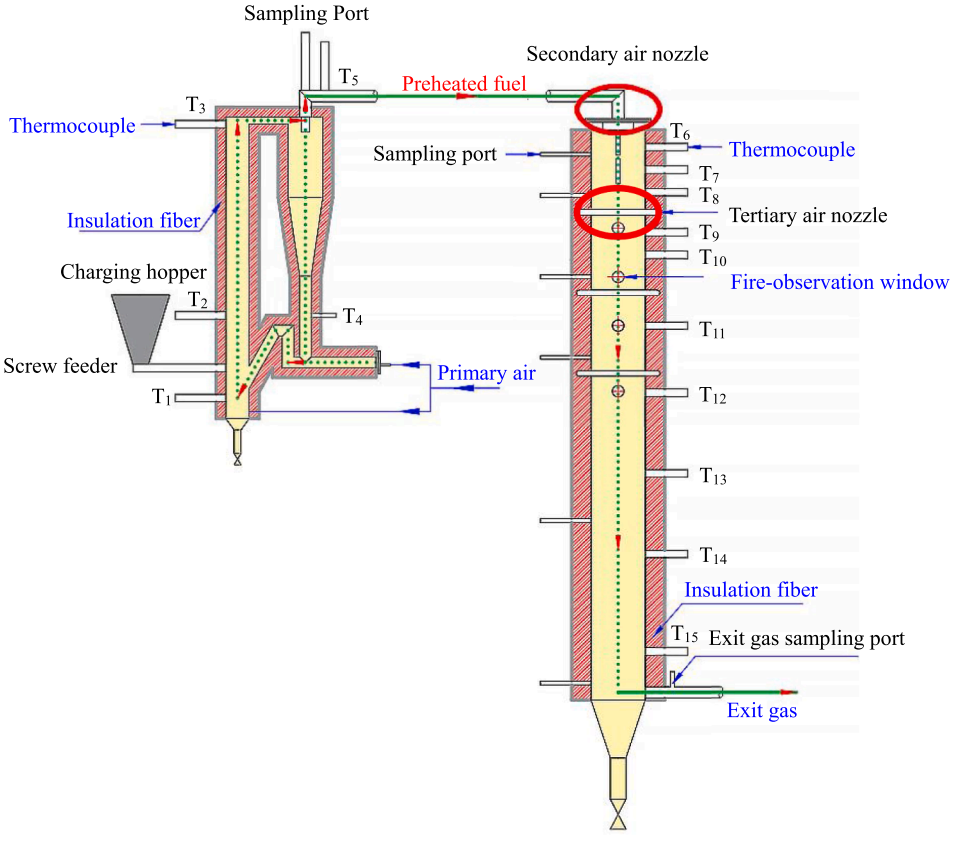

Fig. 1. The Schematic diagram of the self-preheating burner and the down-fired combustor (DFC) in 30 kW pulverized coal flameless combustion system.

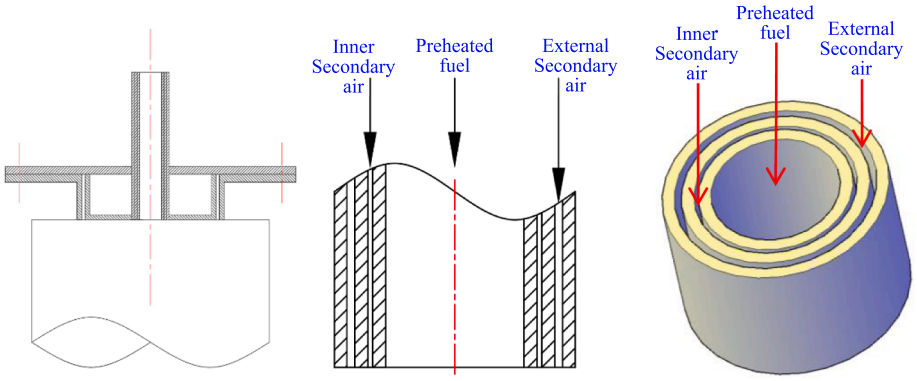

Fig. 2. Schematic diagram of the secondary air nozzle.

schematic diagram of the tertiary air nozzle is shown in Fig. 3.

Six layers of fire-observation windows were set on the side wall of the DFC. Among them, the top two layers were designed with a 15 × 150 mm square structure, and the other four layers were designed in circular structures with an inner diameter of 63 mm. A small amount of compressed air was introduced into these fire-observation windows, facilitating to purge the dust stratification. During this experiment, the total amount of this part of compressed air was extremely small, so its impact on combustion was ignored in this paper. A Ganon G7X digital camera (Canon Inc., Japan) was used to capture the combustion image along the DFC, with camera parameters uniformly adjusted to aperture F4, shutter speed at 1/1000 s, and ISO 1000.

The temperature measurement point distribution is shown in Table 1. The self-preheating burner was equipped with 5 K-type thermocouples, located at the bottom, middle and top of the riser, as well as the back-feeder and the outlet of cyclone separator. Ten S-type thermocouples were arranged down from the preheated fuel nozzle along the centerline of the DFC. Sampling apertures were set at the outlet of the self-preheating burner and at the position of 150 mm, 400 mm, 900 mm, 1400 mm, 2400 mm, and 3400 mm respectively from the top of the DFC to collect solid and gas samples for analysis. A testo-350 flue gas analyzer (Testo AG, Germany, instrument error $< \pm 5\%$) and a zirconia oxygen analyzer were used to measure the oxygen content at the tail of the test system online in order to calculate the equivalence ratio. The fly ash was sampled at the outlet of the flue gas cooler to analyze the carbon content and calculate the combustion efficiency (η). Each case of the experiment conducted in the paper has been running steadily for about 2 h. The temperature fluctuation of each measuring point of the system was controlled within $\pm$ 4 °C during the sampling process.

2.2. Fuel characteristics

The fuel used in the experiments was semi-coke which was the byproduct from the pyrolysis of Shenmu bituminous coal, and its properties (proximate and ultimate analysis) are listed in Table 2. In order to study the influence of different particle size on the preheating and combustion behavior of the fuel, the sieves with four different pore size of 0.1 mm, 0.18 mm, 0.355 mm and 0.5 mm were selected to screen the semi-coke particles before the experiment. Three kinds of Shenmu semi-coke were separated by narrow screens with 0–0.1 mm, 0.1–0.18 mm and 0.18–0.355 mm, while the other three sizes were in a wide sieve: 0–0.18 mm, 0–0.355 mm and 0–0.5 mm. A Mastersizer 2000 laser analyzer was adopted for particle size distribution of Shenmu semi-coke analysis, with 50% cut size (d_{50}) of 35.34 μm, 100.17 μm, 198.54 μm, 45.72 μm, 163.84 μm and 395.63 μm, respectively.

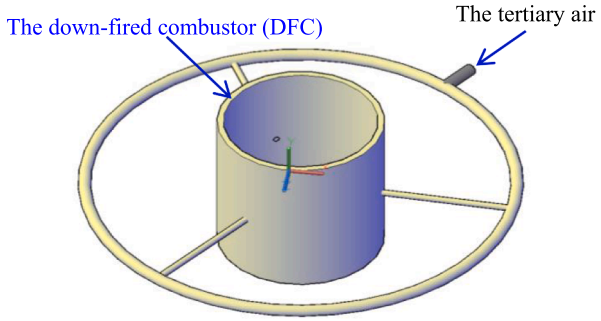

Fig. 3. Schematic diagram of the tertiary air nozzle.

2.3. Experimental conditions

Experimental conditions are listed in Table 3. Except for the difference in fuel particle size, other operating conditions remained unchanged during the experiment. The tertiary air was introduced from 1000 mm below the top of the DFC. In the table, λ_p, λ_2, λ_3 and λ are respectively denoted as the ratio of the primary air flow rate, the secondary air flow rate, the tertiary air flow rate and the total air flow rate to the theoretical combustion air. Two groups of experiments were conducted: the first group (C1-C3) with narrow particle size distribution and the other group (C4-C6) with wide particle size distribution. The thermal load of the test bench was set at about 39 kW. The fuel feed rate was kept constant at 5.20 kg/h and the oxygen concentration at the end of the test system remains within the range of 2.5% ~ 3%.

3. Results and discussion

3.1. The operation characteristics of the self-preheating burner

Fig. 4 shows the temperature profiles of the self-preheating burner with different particle size. It could be seen from the figure that the bulk combustion temperature in the self-preheating burner was the highest when the mean particle size (d_{50}) was 163.84 μm, followed by 35.34 μm, while the preheating temperature of Shenmu semi-coke with d_{50} = 395.63 μm, was the lowest. This difference was relevant to the separation performance of the cyclone separator and the reaction rate of fuel. When the particle size of Shenmu semi-coke was minor and less than 163.84 μm, the separate effect of the cyclone separator would be weakened, and most Shenmu semi-coke passed through the self-preheating burner just for once, leading to a reduction of the combustion share of the Shenmu semi-coke and a decline in the amount of heat released by combustion; When the particle size was too large, especially at d_{50} = 395.63 μm, the specific surface area became smaller, resulting in the slowness of the devolatilization process and heat transfer process. Then the reaction rate was significantly reduced, and the time required to reach equilibrium was extended [34]. Therefore, under the same fuel feed rate condition, the temperature in C5 reached the highest. Additionally, the self-preheating burner operated intensely stably in each

Table 1
Temperature measurement point distribution.

Self-preheating burner										
Thermocouple	T_1		T_2		T_3		T_4		T_5	
Distance From the bottom	100 mm		500 mm		1450 mm		Loop seal		outlet	
Down-fired combustor										
Thermocouple	T_6	T_7	T_8	T_9	T_{10}	T_{11}	T_{12}	T_{13}	T_{14}	T_{15}
Distance from the top (mm)	100	250	400	600	800	1200	1600	2100	2600	3200

Table 2
The properties of Shenmu semi-coke.

Items	Data
Ultimate analysis (*wt. %, air dry*)	
Carbon (C_{ad})	77.60
Hydrogen (H_{ad})	1.24
Oxygen (O_{ad})	4.26
Nitrogen (N_{ad})	0.84
Sulfur (S_{ad})	0.36
Proximate analysis (*wt. %, air dry*)	
Moisture (M_{ad})	6.64
Ash (A_{ad})	9.06
Volatile matter (V_{ad})	8.45
Fixed carbon (FC_{ad})	75.85
Low heating value (MJ/kg)	27.03

case of the experiment, with the highest temperature in dense phase zone (T_2) and the lowest temperature at the bottom of the riser (T_1).

3.2. Particle size distribution of the coal char

The particle size was analyzed after collecting coal char at the outlet of the self-preheating burner. Fig. 5 shows the particle size distribution of coal char with different particle size. The hollow symbol represents Shenmu semi-coke and the solid symbol stands for coal char. It was speculated that the smaller particles were directly consumed by thermal decomposition while the larger particles were burned and broken in the self-preheating burner, resulting in the highest proportion of the medium-size particles. After being preheated by the self-preheating burner, the particle size range of the coal char was almost in the range of 0–100 μm. Compared with Shenmu-semi-coke, the particle size of coal char was significantly decreased, leading to a better reactivity and the improved combustion performance [35]. Furthermore, the difference of particle size between Shenmu semi-coke and coal char became smaller if Shenmu semi-coke particle size was smaller.

3.3. Particle structure and characteristics of the coal char

The gas adsorption method, with N_2 as the adsorptive at 77 K, was applied to analyze the pore structure of Shenmu semi-coke and coal char. The Micromeritics ASAP 2460 Surface Area and Porosimetry Analyzer (U. S.) was used. The specific surface area was determined by the Brunauer Emmett Teller (BET) theory [36], and the pore size distribution, calculated by The Barrett Joyner Halenda (BJH) theory [37], was also provided. Fig. 6 shows the changes in specific surface area of Shenmu semi-coke with different particle size. After Shenmu semi-coke was preheated by the self-preheating burner, the specific surface area was significantly increased. The surface became rough with a well-developed pore structure, leading to the improvement of physical structure of the high-temperature preheated fuel particles, which was consistent with Ouyang's results [25,35]. When d_{50} = 163.84 μm (Fig. 4), the specific area of Shenmu semi-coke increased significantly the most, from the original 3.18 m^2/g to 166.95 m^2/g. Additionally, it can also be seen from the figure that the effect of physical action (grinding) on the specific area of Shenmu semi-coke was far less than that of chemical action (pyrolysis/ gasification).

Fig. 7 shows the changes in average pore diameter of Shenmu semi-coke with different particle size. Different from the changes in specific surface area, the average pore diameter of coal char was reduced in comparison with Shenmu semi-coke, and the regularity of changes in average pore diameter became more obvious that the degree of decline became smaller and smaller with the increase in Shenmu semi-coke particle size. When d_{50} = 35.34 μm, the difference was the maximum (6.68 nm); When d_{50} = 395.63 μm, the difference was the minimum (0.68 nm). Howard and Essenhigh [38] pointed out that the particles

Table 3
Experimental conditions.

Items	Unit	C1	C2	C3	C4	C5	C6
Size distribution	–	Narrow			Wide		
Particle size	mm	0–0.1	0.1–0.18	0.18–0.355	0–0.18	0–0.355	0–0.5
d_{50}	μm	35.34	100.17	198.54	45.72	163.84	395.63
Thermal load	kW	39.04	39.04	39.04	39.04	39.04	39.04
Fuel feed rate	kg/h	5.20	5.20	5.20	5.20	5.20	5.20
M_1	Nm^3/h	12.37	12.37	12.37	12.37	12.37	12.37
λ_P	–	0.33	0.33	0.33	0.33	0.33	0.33
M_{21}	Nm^3/h	10.29	10.29	10.29	10.29	10.29	10.29
M_{22}	Nm^3/h	9.66	9.66	9.66	9.66	9.66	9.66
λ_2	–	0.53	0.53	0.53	0.53	0.53	0.53
M_3	Nm^3/h	10.80	10.80	10.80	10.80	10.80	10.80
λ_3	–	0.29	0.29	0.29	0.29	0.29	0.29
M	Nm^3/h	43.12	43.12	43.12	43.12	43.12	43.12
λ	–	1.15	1.15	1.15	1.15	1.15	1.15

Notes:
M_1-Primary air flow (m^3/h)
M_{21}-Inner secondary air flow (m^3/h)
M_{22}-External secondary air flow (m^3/h)
M_3-Tertiary air flow (m^3/h)
M-Total combustion air flow (m^3/h)

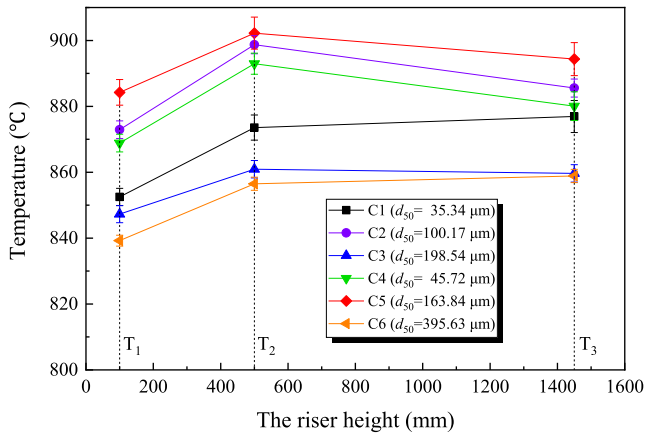

Fig. 4. Temperature profiles of the self-preheating burner with different particle size.

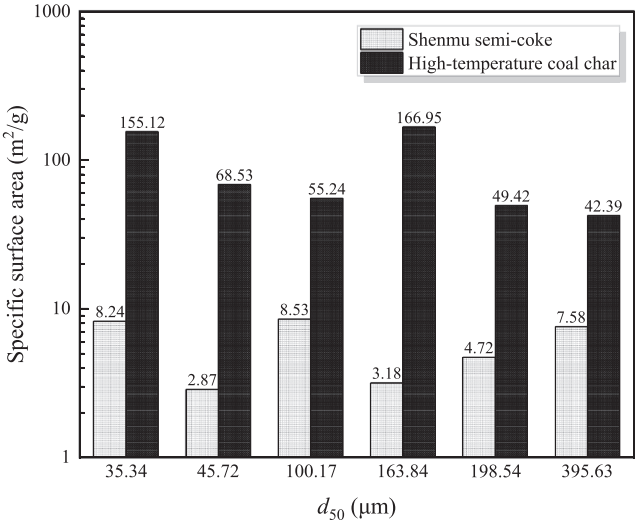

Fig. 6. Changes in specific surface area of Shenmu semi-coke and the high-temperature coal char in C1-C6.

would soften into spheres and expand into porous forms in the course of pulverized coal combustion, and different types of fuel would lead to different variations of pore structure in devolatilization process. What's more, the average pore diameter of fuel preheated in the self-preheating burner became more complex than conventional combustion. For Shenmu semi-coke, the strong thermal shock in the self-preheating burner obviously influenced its particle breakage, resulting in the changes of the internal pore structure. In this study, the average pore diameter decreased after Shenmu semi-coke was preheated by the self-preheating burner, indicating that there were more of the larger pore disappearing, which was unfavorable to improve the combustion characteristics of coal char. However, the degree of decline in average pore diameter was much more minor than that of increase in specific surface area.

Fig. 8 shows the changes in total pore volume of Shenmu semi-coke with different particle size. Besides the specific surface area, the pore volume of coal char also increased obviously in comparison with Shenmu semi-coke after being preheated. For the reason that most volatiles were precipitated in the preheating process of Shenmu semi-coke, leading to the formation of a large number of new pores inside and on the surface of the coal char particles, thus the pore structure became developed, making the total pore volume of the particle larger, which was conducive to the contact and combination of coal char and O_2

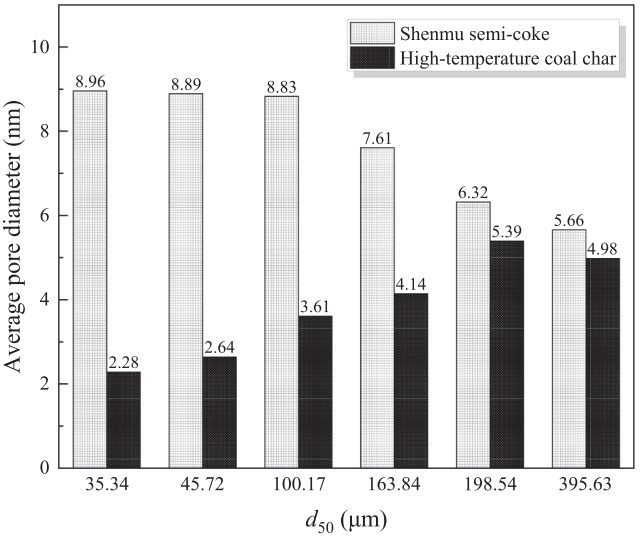

Fig. 7. Changes in average pore diameter of Shenmu semi-coke and the high-temperature coal char in C1-C6.

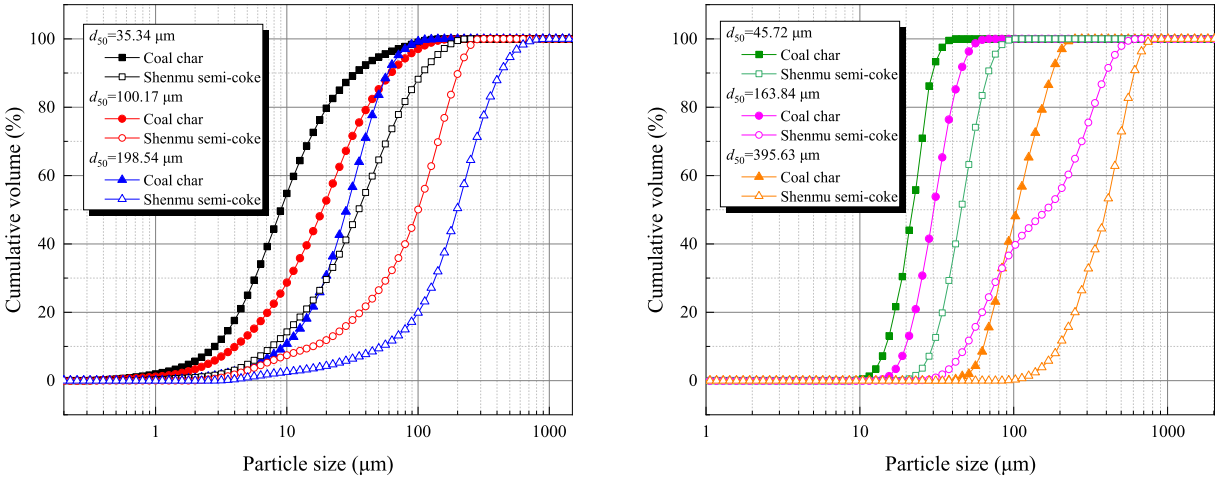

(a) Narrow (b) wide

Fig. 5. Particle size distribution of Shenmu semi-coke and coal char with different particle size.

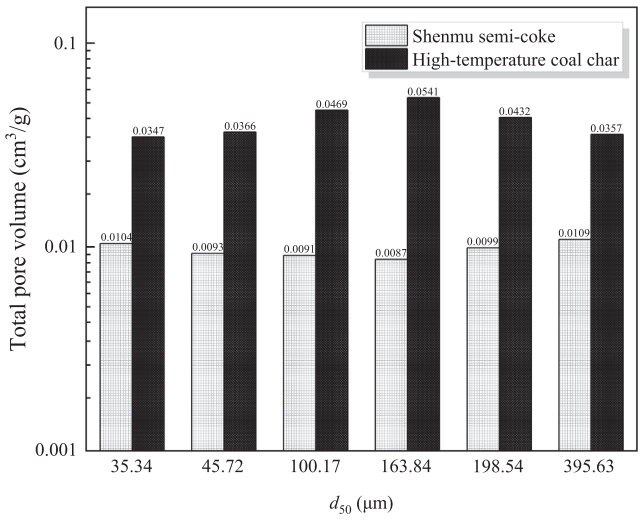

Fig. 8. Changes in total pore volume of Shenmu semi-coke and the high-temperature coal char in C1-C6.

in the subsequent combustion process. The pore volume of coal char increased at the beginning and subsequently decreased with the augment of the particle size of Shenmu semi-coke, and reached its maximum value at $d_{50} = 163.84$ μm. It could be speculated that Shenmu semi-coke with different particle size might result in different action of thermal stress and friction in the process of preheating [35], thus bringing about the difference of total pore volume of coal char.

Therefore, the comprehensive comparison of the above various physical indicators of high-temperature coal char showed that preheating played an important role in improving the physical structure of Shenmu semi-coke. The physical index of the high-temperature coal char had the best improvement effect when d_{50} was 163.84 μm (0–0.355 mm), suggesting that the combustion effect of such coal char after entering the DFC from the cyclone separator could reach optimal efficiency.

3.4. Discussion about preheating characteristics in the preheating burner

The gas at the outlet of the self-preheating burner was collected by an air bag to analyze its composition with an Agilent 3000A Micro GC (the sensitivity was less than 10–20 ppm and the instrument error was within ± 2%) equipped with a thermal conductivity detector. Fig. 9 shows the coal gas compositions of Shenmu semi-coke with different particle size (dry basis). The highest composition in the high-temperature coal gas was N_2 (all above 70%), implying that more fuel bound N could be better released from volatile matter and converted into N_2 in the self-preheating burner [7,25]. The content of H_2 and CH_4 were the highest when $d_{50} = 163.84$ μm, nevertheless CO reached the lowest (Fig. 9d). But when $d_{50} = 395.63$ μm, the high-temperature coal gas composition (H_2, CH_4 and CO) was just the opposite (Fig. 9f). In combination with Fig. 4, the combustion temperature in the self-preheating burner reached the highest value at $d_{50} = 163.84$ μm and the lowest value at $d_{50} = 395.63$ μm, suggesting that with the increase of the preheating temperature, the yield of H_2 beefed up, while the yield of CO was just the opposite. For the trigger that when the combustion temperature increased, in comparison to the Boudouard reaction ($C + CO_2 = 2CO$), the water–gas shift reaction ($CO + H_2O = CO_2 + H_2$) dominated, leading to the generation of H_2 and consumption of CO [39].

In addition to the main components of coal gas, other trace gases (ppm level) were also measured in this experiment. Made free of interferences from any other gas, the concentrations of NH_3 and HCN were measured by DOAS and LasIR^{TM} Gas Analyzer (Unisearch Associates Inc) since the spectral purity was high and the selected absorption feature was unique. And NO, NO_2 and O_2 were detected by KM9106 portable flue gas analyzer. The test results are shown in Fig. 10. The results revealed that NO, NO_2 and O_2 were not detected in the coal gas, indicating that the coal gas was in strong reduction and had a good inhibitory effect on the generation of NO_x [7]. In terms of nitrogenous gas, the concentration of NH_3 was second only to N_2, and the yield increased first and then decreased with the augment of the particle size of Shenmu

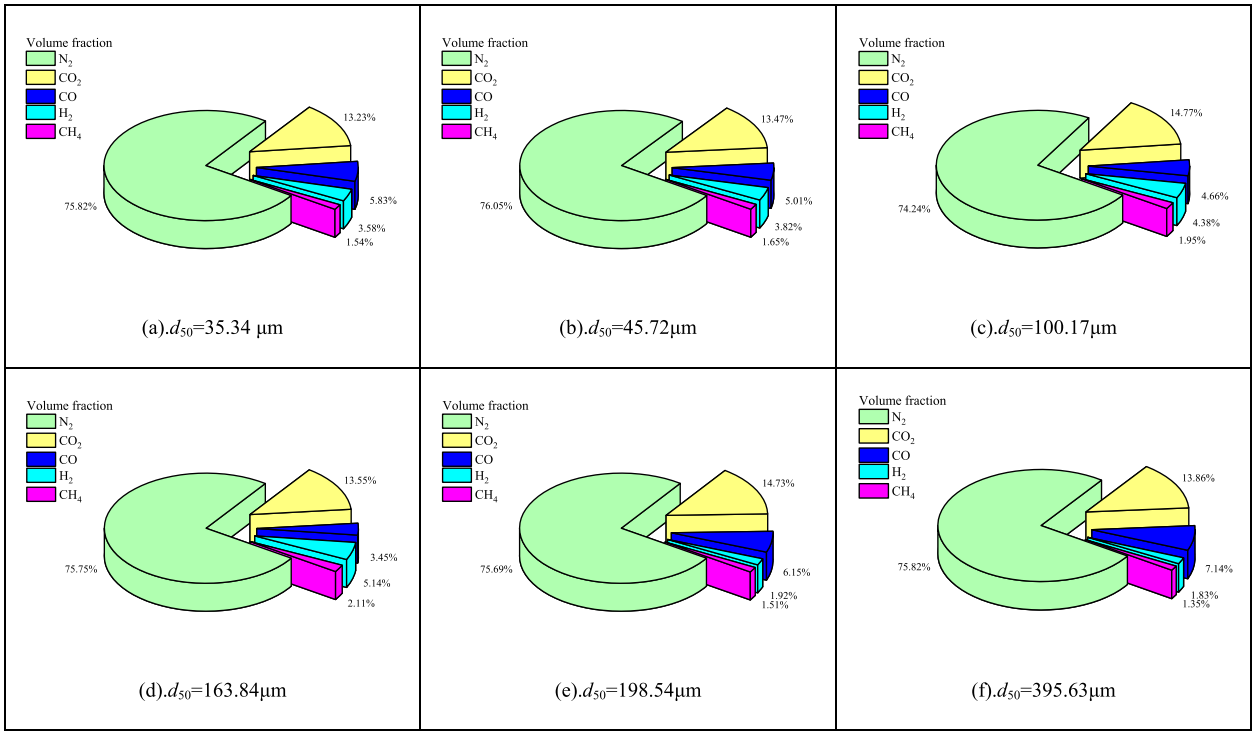

Fig. 9. Coal gas compositions of Shenmu semi-coke with different particle size (dry basis).

semi-coke, reaching the maximum at $d_{50} = 163.84$ μm. The yield of HCN decreased with the increase of the particle size of Shenmu semi-coke, but the content was so minor that it could be negligible. This meant in terms of nitrogenous gas, only NH_3 was sent into the DFC for continued combustion and became one of the major precursor of NO_x (N_2 did not participate with reactions). Therefore, it could be concluded that most of the released fuel bound N was converted into N_2 and NH_3, which was advantageous to control the overall NO_x emissions of the system.

Table 4 shows the proximate and ultimate analysis of coal char of Shenmu semi-coke with different particle size. The conversion rate of a substance was defined as the ratio of the total amount of a component released into the flue gas to the total amount of that component in Shenmu semi-coke. Hence the ash balance hypothesis was obtained: 1) The ash in the fuel did not participate in the reaction during the combustion process; 2) No new ash content was generated during the combustion process, that was, ash content kept unchanged in the course of the entire process. The conversion rate calculation formula was as follows [40]:

$$C_x = 1 - \frac{A_1 X_2}{A_2 X_1} \quad (1)$$

where A_1 and A_2 are respectively the ash content of Shenmu semi-coke and the coal char (%), X_1 and X_2 represent the content of element or component x of Shenmu semi-coke and coal char (%), respectively.

Based on ash balance hypothesis, the conversion rate of each component in Shenmu semi-coke can be calculated, and the results are shown in Fig. 11. When $d_{50} = 100.17$ μm, the conversion rate of each component (C, H, N and V) was the highest during the self-preheating combustion process, all exceeding 70%. While the lowest conversion rate of each component was reached at $d_{50} = 395.63$ μm. When $d_{50} = 100.17$ μm, the fuel bound N and volatile matter were released in almost equal proportion, while the conversion rate of fuel bound N in the other five types of Shenmu semi-coke particles were obviously lower than that of volatile matter, especially at $d_{50} = 395.63$ μm and $d_{50} = 198.54$ μm, suggesting that the high-temperature coal char of Shenmu semi-coke particles still had nearly half of the fuel bound N remained, which would be the main source of NO_x in the subsequent combustion. On the whole, as increasing d_{50}, the conversion rate of each component increased at the early stage and then decreased. When d_{50} increased from 35.34 μm to 100.17 μm, the conversion rate of each component increased, but the increment was not obvious enough; When further increased to 395.63 μm, the conversion rate of each component decreased significantly.

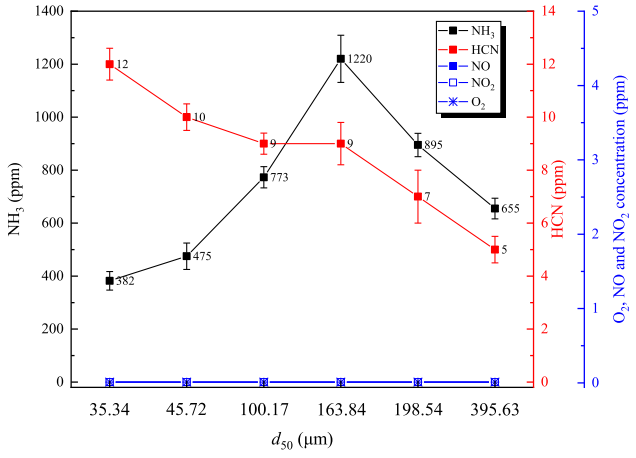

Fig. 10. O_2 and other nitrogenous gas concentrations in the high-temperature coal gas.

Table 4
Proximate and ultimate analysis of the coal char for Shenmu semi-coke with different particle size.

Items	C1	C2	C3	C4	C5	C6
d_{50} (μm)	35.34	100.17	198.54	45.72	163.84	395.63
Ultimate analysis (wt. %, air dry)						
Carbon (C_{ad})	70.94	64.48	74.86	62.43	66.84	75.89
Hydrogen (H_{ad})	1.11	0.95	1.49	0.98	1.17	1.52
Oxygen (O_{ad})	1.47	1.05	1.89	1.37	1.66	1.93
Nitrogen (N_{ad})	1.01	0.67	0.99	0.70	0.78	1.02
Sulfur (S_{ad})	0.51	0.50	0.56	0.55	0.56	0.51
Proximate analysis (wt. %, air dry)						
Moisture (M_{ad})	1.47	1.12	1.60	1.88	1.44	1.62
Ash (A_{ad})	23.49	31.23	18.61	21.33	20.46	18.75
Volatile matter (V_{ad})	7.97	6.65	7.28	5.84	6.27	7.62
Fixed carbon (FC_{ad})	67.07	61.02	72.51	70.95	71.83	71.25

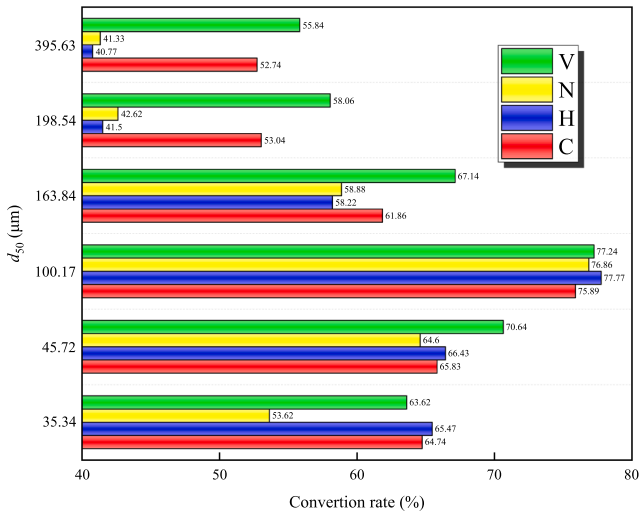

Fig. 11. Conversion rates of the components of coal char for Shenmu semi-coke with different particle size.

3.5. Combustion characteristics of the high-temperature preheated fuel

Fig. 12 shows the temperature profiles of the DFC for Shenmu semi-coke with different particle size. Under different conditions, the curves have basically the same variation trend: reduce first and then ascend, all reaching the peak value at 800 mm and gradually attenuating and approximating straight lines below 1200 mm. Except for $d_{50} = 163.84$ μm, the overall combustion temperature gradually decreased with the increase of Shenmu semi-coke particle size. The sums of combustible gas components in the high-temperature coal gas were similar in different cases (Fig. 9), therefore the temperature of the area below the preheated fuel nozzle exit differed little. However, the high-temperature coal char had longer combustion process and slower combustion rate. For $d_{50} = 163.84$ μm particle, the specific surface area and pore volume of coal char were both the largest (Figs. 6 and 8), thus the preheated coal char could be well mixed with the combustion air after entering the DFC, leading to the highest combustion temperature. Additionally, when $d_{50} = 35.34$ μm, the coal char had the smallest particle size and the second highest specific surface area (Figs. 5 and 6), thus the combustion temperature was second only to that of $d_{50} = 163.84$ μm. While the coal char had the largest particle size and the smallest specific surface area when $d_{50} = 395.63$ μm, resulting in the lowest combustion temperature and the slowest reaction rate. For these six cases, the maximum temperature in the DFC was all lower than 1100 °C, indicating that the output of thermal NO_x was extremely low that could be almost negligible, hence

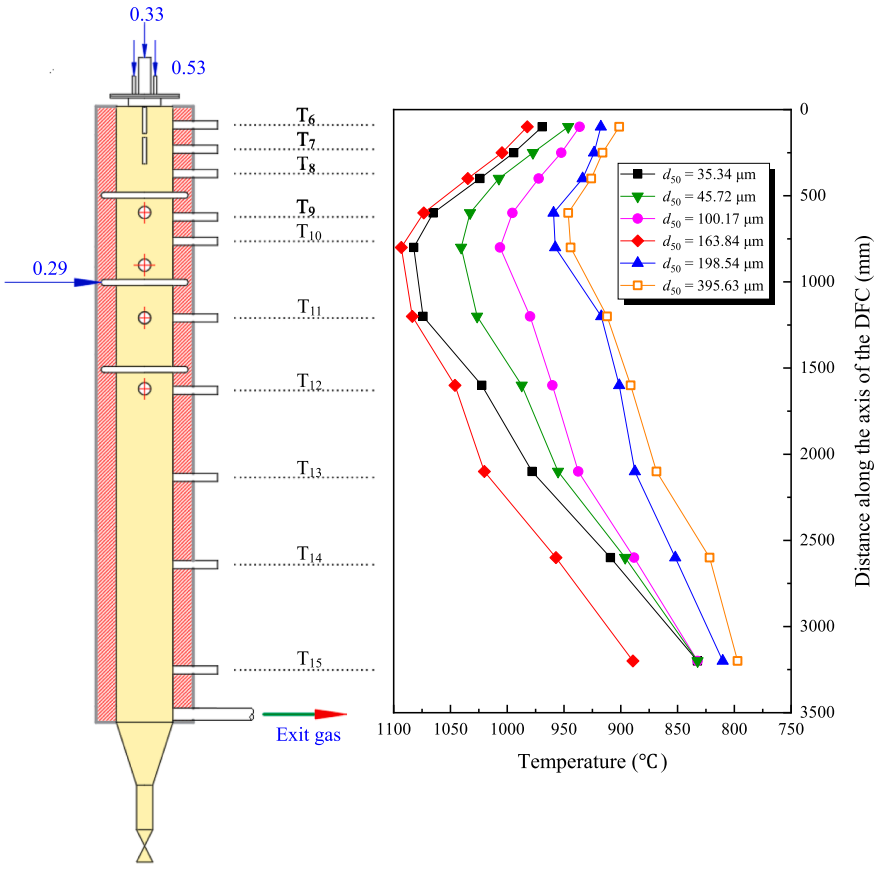

Fig. 12. Temperature profiles of the DFC for Shenmu semi-coke with different particle size.

the NO_x generated in this experimental study was mainly fuel NO_x.

Fig. 13 shows the flame images along the DFC of Shenmu coke with different particle size. In general, the brightness of the image at the same location was proportional to the combustion temperature. As can be seen, except for d_{50} = 163.84 μm, the brightness of the entire combustion zone became increasingly dimmed with the increase of Shenmu semi-coke particle size, relatively consistent with the temperature distribution trend of the DFC (Fig. 12). Especially when d_{50} = 395.63 μm, through fire-observation windows, the top area of the DFC was almost vague and even invisible, but some bright spots (traces of small solid particles burning) scattered in the middle combustion area. Although the temperature at the top of the DFC was all above 900 °C, the flame images basically appeared as dark color with lower brightness. The possible reason was the recirculation and backflow of the high-temperature coal gas which mainly burnt at the top of the DFC while the downstream was mainly for the combustion of coal char. Their intensity of visible light emitted during combustion progress were different. It was seen that the combustion area was transparent and no visible front flame existed, additionally, the nozzle and some thermocouples could be clearly observed. Combined with the temperature profiles of the DFC (Fig. 12), it could be judged that all cases had achieved flameless combustion (a phenomenon, not a specific combustion technology, but a consequence of the way combustion was organized).

The fly ash at the outlet of the flue gas cooler in different cases was all collected. According to the literature [40], combustion efficiency (η), which was defined as the ratio of heat released by the incomplete combustion of fuel to heat released by complete combustion of fuel, were computed in accordance with the detailed equations (7) to (9). Fig. 14 shows combustion efficiencies (η) of Shenmu coke with different particle size. When d_{50} = 163.84 μm, the specific surface area and pore volume of coal char were the largest (Figs. 6 and 8), resulting in an optimal mixture of coal char and combustion air. Therefore the highest η (98.23%) was reached at this point, with the brightest flame image (Fig. 13) and highest temperature (Fig. 12). Except for d_{50} = 198.54 μm and 395.63 μm, the other η were all exceeding 96%, which meant and proved that too large fuel particle size would lead to the deteriorated combustion, significantly reducing the combustion efficiency.

3.6. Flue gas analysis

A Fourier infrared gas analyzer (Gasmet Technologies Oy, Finland, instrument error < ± 2%) was used to measure the compositions of the flue gas along the axis of the DFC online. Fig. 15 shows CO_2, O_2 and CO concentration along the DFC. Evenly distributed with a peak value less than 6%, the concentration of O_2 increased at first, and then begun to descend (Fig. 15b), while the concentration of CO_2 tended to the opposite direction of O_2 concentration (Fig. 15a). Low O_2 concentration in the combustion zone is beneficial to inhibit the generation of NO_x. The lowest concentration of CO_2 occured at 900 mm. In the high-temperature coal gas, the concentrations of CO_2 were all less than 15% (Fig. 9), but the CO_2 concentration near the preheated fuel nozzle exit was significantly higher than this value. Therefore, it could be inferred that the high concentration of CO_2 here was supposed to be caused by the rapid ignition of coal gas (especially CO) and flue gas recirculation after the preheated fuel left the self-preheating burner and entered the DFC that had higher temperature. After the gradual mixing of preheated fuel and combustion air, the subsequent decrease of CO_2 concentration was due to the dilution of gas concentration because of the dispersion of combustion reaction in a large space. Due to the introduced tertiary air, more CO was oxidized by O_2, resulting in the increase of CO_2 concentration below 900 mm. What's more, the oxygen concentration fluctuates slightly below 1500 mm and the combustion area continues to expand, helping to make the temperature in the combustion area more uniform and reduce the peak temperature. The

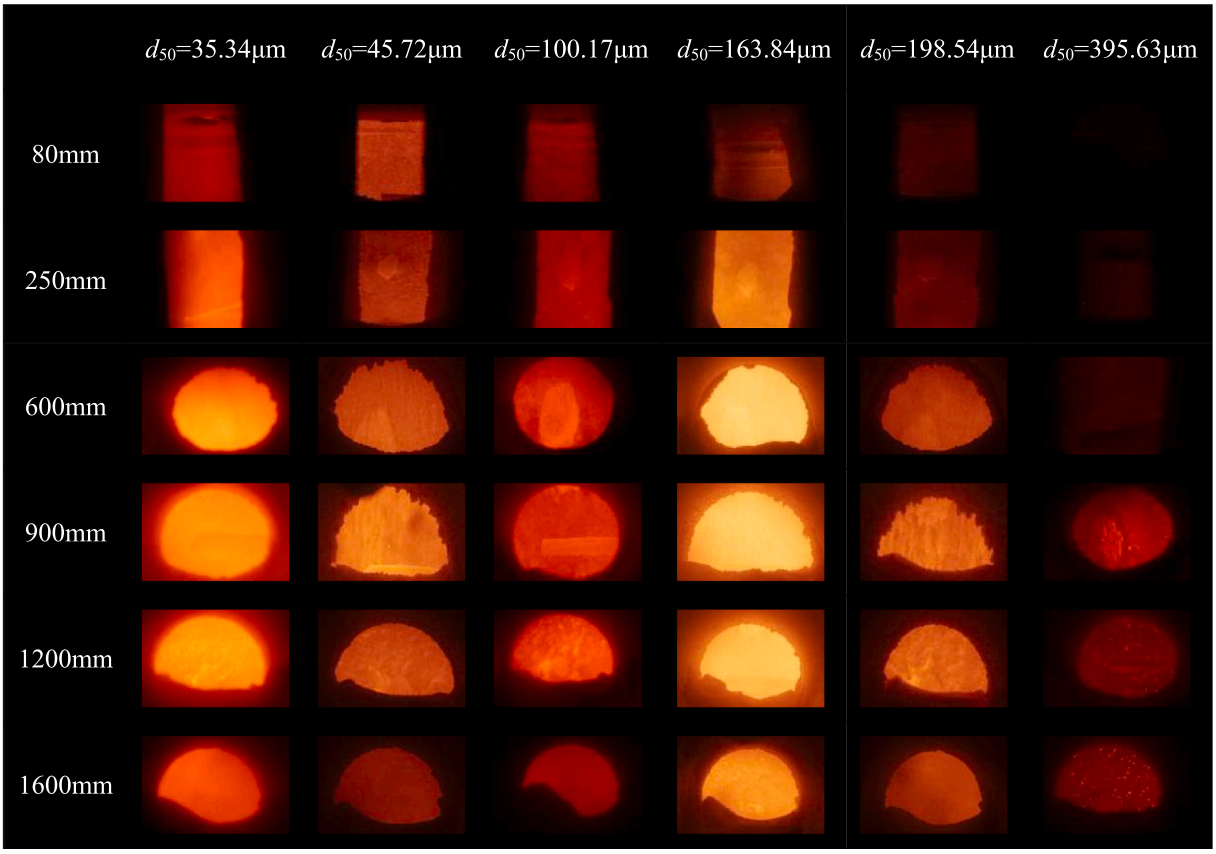

Fig. 13. Flame images along the DFC of Shenmu coke with different particle size.

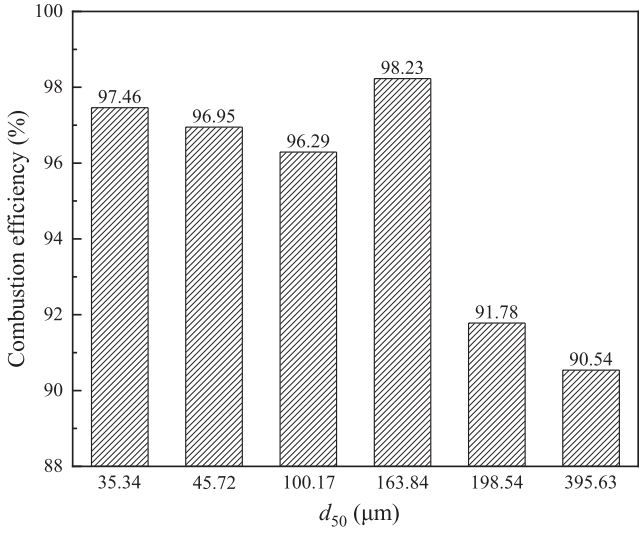

Fig. 14. Combustion efficiencies (η) of Shenmu semi-coke with different particle size.

contact time between NO and CO was prolonged in the meanwhile, which is conducive to the reduction of NO. When the concentration of CO_2 and O_2 did not change significantly, the combustion reaction had been reduced enough. Since changes in O_2 and CO_2 concentrations can also reflect the intensity of combustion to some extent, it could be concluded that when other conditions remain unchanged, the size of the preheated fuel combustion zone and the combustion intensity would change significantly due to the difference of Shenmu semi-coke particle size.

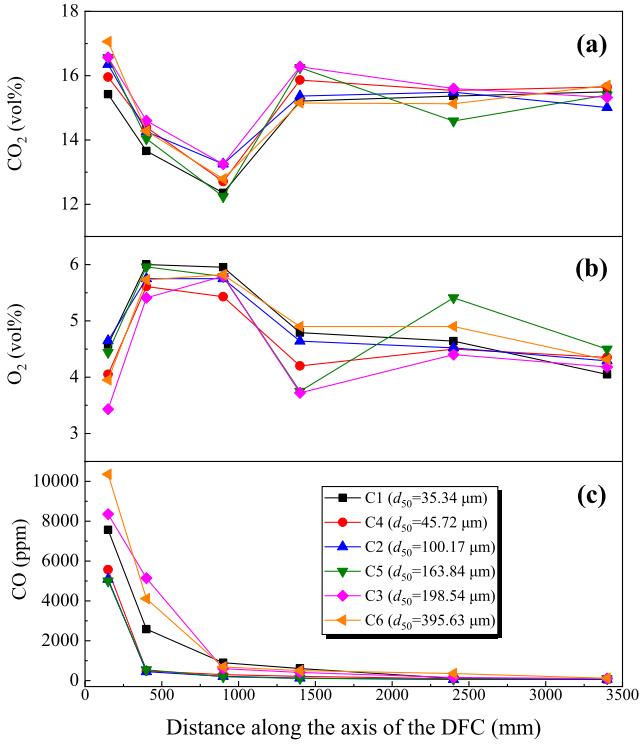

Fig. 15. CO_2, O_2 and CO concentrations along the DFC of Shenmu semi-coke with different particle size.

After Shenmu semi-coke with six different particle size was

preheated and passed through the self-preheating burner, CO was generated and subsequently entered the DFC from the cyclone separator. As can be seen from Fig. 15c, the initial concentration and the decline range of CO increased with d_{50}. In the 0 ~ 900 mm area, the concentration of CO at the first measurement point was higher, and then quickly consumed to a lower level from more than 5% to 0.5% or even less, which implied that the main combustion zone of CO was range from 0 mm to 900 mm, because CO and the secondary air met each other and reacted with O_2 to produce more CO_2. Unlike the coal char, the coal gas first ignited and burned rapidly in a narrow combustion zone, while coal char diffused into a large space and burned slowly. It could be concluded that the high-temperature coal gas was almost exhausted before the tertiary air was introduced, and the area below the tertiary air nozzle was the burn-out zone of the remaining char. The rate of CO produced by coal char combustion was slightly lower than that of CO consumption in coal gas, making CO concentration decreased gradually.

Fig. 16 shows concentrations of various gases containing nitrogen along the DFC of Shenmu semi-coke with different particle size. HCN is an unstable component that can be further oxidized at high temperature. Miller and Bowman [41] considered the reaction mechanism of HCN converting to NO and N_2 through the calculation of reaction kinetics model and the comparison of experimental results. In this study, the combustion temperature in the DFC was high and the fuel was dispersed in a large reducing atmosphere, giving rise to the diffuse distribution and low concentration of oxygen, thus HCN was more likely to be directly converted into N_2 [42].

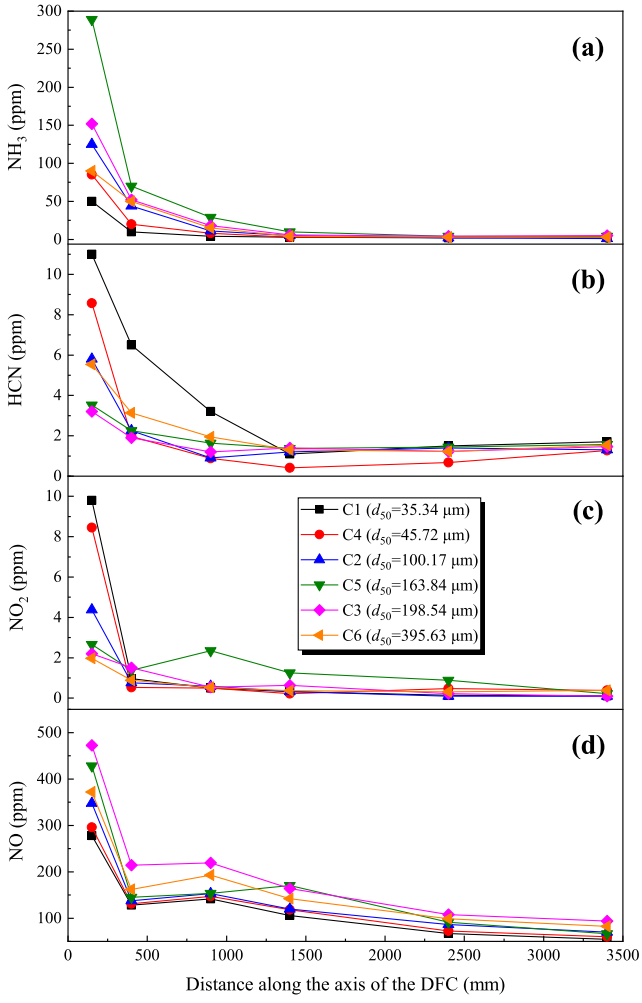

Fig. 16. Concentrations of various gases containing nitrogen along the DFC of Shenmu semi-coke with different particle size.

Widely used in power plants to reduce NO_x emissions, NH_3, on the other hand, was a good NO_x inhibitor. In the reducing atmosphere, injecting NH_3 into the flue gas was an effective way to reduce NO_x emissions. By comparing Fig. 16a and b, the concentration of NH_3 changed at a faster rate than that of HCN, indicating that NH_3 had a better reactivity. When $d_{50} = 163.84$ μm, NH_3 concentration reached the highest due to the maximum content in the coal gas (Fig. 10). In each case, the curves of NH_3 and HCN concentration all dropped sharply to nearly zero in the low-oxygen DFC where NH_3 had certain reducing property, which could promote NO_x reduction to N_2. The main reduction reaction [43] involved was:

$$\boldsymbol{NH_3 + H \rightleftharpoons NH_2 + H_2} \quad \text{(R1)}$$

$$\boldsymbol{NH_2 + NO \rightleftharpoons N_2 + H_2O} \quad \text{(R2)}$$

NO_2 was one of a highly reactive gas known as oxides of nitrogen (NO_x). It began to decompose when the temperature was higher than 150 °C, and almost completely decomposed to NO and O_2 when the temperature reached 650 °C. As a consequence, under the high-temperature condition of the DFC, NO_2 concentration measured at each measurement point was relatively low and NO_x in the DFC was mainly presented in the form of NO. In Courtemanche' s research [44], NO_2 emission was found in the post-flame oxidation zone, often accompanied by the conversion to NO. The main generation and consumption reactions for NO_2 were as follows:

$$NO + HO_2 = NO_2 + OH \quad \text{(R3)}$$

$$O + NO_2 = NO + O_2 \quad \text{(R4)}$$

$$H + NO_2 = NO + OH \quad \text{(R5)}$$

NO was rapidly generated after the preheated fuel was mixed well with the secondary air. The changing trends of NO at different Shenmu semi-coke particle size were basically consistent: 1) The generated NO concentration decreased rapidly within the range of 150 mm to 400 mm; 2) But in the range of 400 mm to 900 mm, the generated NO concentration increased slightly; 3) Below 900 mm of the DFC, the concentration of NO turned to a decline again but slowly. The rapid decrease of NO concentration at the beginning was contributed to the reducing coal gas and coal char. Additionally, the subsequent increase of NO concentration was caused by the oxidation of nitrogen-containing substances due to the introduction of tertiary air. Below 900 mm of the DFC, the slow decline of NO concentration should be the consequence of the reduction of solid char as coal gas had been basically consumed. Therefore, in the combustion process of the DFC, the char exerted a decisive part in NO reduction due to the longer reduction time of the char to NO than the homogeneous reduction time between gases.

Fig. 17 shows NO_x and CO emissions of Shenmu semi-coke with different particle size. All data have been converted to the standard value at 6% oxygen concentration (@6% O_2). In Glarborg' s reaesrch [45], CO in the pure gaseous state was very difficult to react with NO. Additionally, H_2 and CO had no effect on NO reduction under 1400 K, but CO could be used as catalyst to promote the NO-char reaction. The reaction between CO and NO was primarily concentrated at the top of the DFC, while the reaction between coal char particles and NO was mainly in the middle and lower part (Fig. 15). In Fig. 17, the relationship between CO and NO became not particularly obvious, because NO_x and CO emissions have been relatively low under all cases, indicating that the preheating combustion technology could combined with particle modification, combustion control and fractional combustion technology, so as to achieve the organic integration of high efficiency combustion and low NO_x emissions. The exit NO_x emission was minimized at d_{50} = 35.34 μm (89.46 mg/m^3) and maximized at d_{50} = 198.54 μm (148.53 mg/m^3). As for the effect of particle size on NO_x formation during combustion, some previous studies [31,46–51] have also been carried out. On a small text rig, Okazaki [46] and Kramlich [47] found

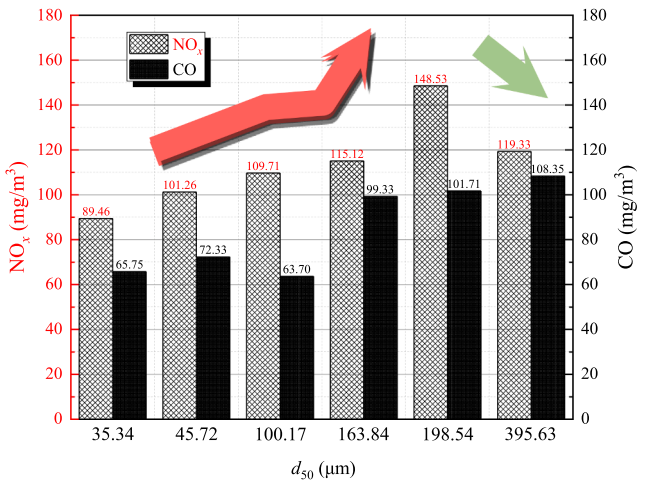

Fig. 17. NO_x and CO emissions of Shenmu semi-coke with different particle size.

that the smaller the pulverized coal size was, the higher the NO_x produced by combustion would be. In Smoot's research [48], pulverized coal size had a significant effect on combustion efficiency but little effect on NO_x emissions. Ref. [31] refered that when air staging was not adopted, NO_x emissions concentration increased linearly with the decrease of pulverized coal particles, nevertheless, after using air staging combustion, NO_x emissions concentration could be hardly influenced. Some researchers [46,49,50] held that finer fuel particles would produce more NO_x in the course of their combustion process due to their fast devolatilization and ignition, however, Kamal et al [51]. drew an exact opposite conclusion through their research. Therefore, from the basis of current studies, no unified conclusion about the effect of fuel with different particle size on NO_x emission has been reached on. It was discovered in this experimental that there was a critical value (d_{50} = 198.54 μm) of Shenmu semi-coke particles. When the particle size was lower than or higher than the critical value, NO_x generated by combustion would decrease, which accorded closely with Abbas's results [33]. Virtually, the influencing factors of NO_x emissions are various and complex, including the reactivity of fuel itself, the residence time in the reduction zone of reactor, the combustion temperature and the degree of blending of the reactants. The combustion characteristic and the reactivity of fuel were converted by altering the particle size, which indirectly influenced NO_x emissions. But provided that other methods were used at the same time, such as air staging combustion and self-preheating combustion technology, the effect of fuel particle size on NO_x emissions might be weakened otherwise show the opposite trend.

In a word, to minimize the NO_x emissions, the fuel particle size is set to ensure that the high temperature coal char has a high reactive activity and a improved combustion performance under the premise of reasonable air distribution. As shown above, case 1 provides with the optimal design conditions while considering both the combustion efficiency and the NO_x emissions, for the NO_x emissions are the least and the efficiency is higher than 97%.

4. Conclusions

Experimental researches were carried out on a bench-scale coal self-preheating combustion test apparatus, and six different particle sizes of Shenmu semi-coke (quenching after the pyrolysis of shenmu bituminous coal) were used as fuel to conduct relevant exploratory experiments. The difference of fuel particle size greatly affected the yield of each component in high-temperature coal gas, and the reactive activity of coal char, thus subsequently influenced the final combustion process and NO_x emissions. The behavior characteristics of combustion (self-preheating and flameless) in the entire process and pollutant formation regularity were discussed in detailed. The relevant results are summarized as:

After being preheated in the self-preheating burner, the particle size range of coal char in the six cases were all significantly decreased, besides the specific surface area and pore volume of Shenmu semi-coke were both significantly increased, especially at d_{50} = 163.84 μm, leading to the better reactivity and the improved combustion performance. The difference of particle size between Shenmu semi-coke and coal char became smaller if the particle size of Shenmu semi-coke was smaller.

The bulk preheating temperature of medium-size particles were higher, which was relevant to the separation performance of the cyclone separator and the reaction rate of fuel. If the particle size of Shenmu semi-coke was minor, the separate effect of the cyclone separator would be weakened, leading to a reduction of the combustion share and a decline in the amount of heat released by combustion. If the particle size was too large, the specific surface area became smaller, resulting in the slowness of the devolatilization process and heat transfer process. Then the reaction rate was significantly reduced, and the time required to reach equilibrium was extended.

Fuel with different particle size would lead to the difference of coal gas compositions. Most volatile matter and fuel bound N were separated out in the process of preheating, and the released N was mainly converted to N_2 and NH_3 due to the strong reduction in the self-preheating burner. The different particle size of Shenmu semi-coke resulted in different preheating temperature, which further affected the content of each component in the high-temperature coal gas: with the increase of the combustion temperature in the self-preheating burner, the yield of H_2 beefed up, while the yield of CO was just the oppsite.

When d_{50} = 100.17 μm, the conversion rate of each component (C, H, N and V) was the highest in the self-preheating burner, and the fuel bound N and volatile matter were released in almost equal proportion, while the conversion rate of fuel bound N in the other five types of particles were obviously lower than that of volatile matter, suggesting that the high-temperature coal char still had nearly half of the fuel bound N remained, which would be the main source of NO_x in the subsequent combustion.

The maximum combustion efficiency was 98.23% at d_{50} = 163.84 μm with the brightest flame image and highest temperature. Except for d_{50} = 163.84 μm, with the increase of Shenmu semi-coke particle size, the overall combustion temperature gradually decreased and the brightness of the entire combustion zone became dimmer. Through fire-observation windows, it could be judged all experimental conditions in this study achieved flameless combustion, with a transparent combustion area, but no flame front visible to the naked eye.

It was discovered in this experimental that there was a critical value (d_{50} = 198.54 μm) of Shenmu semi-coke particles. When the particle size was lower than or higher than the critical value, NO_x generated by combustion would decrease. The exit NO_x emission was minimized at d_{50} = 35.34 μm (89.46 mg/m^3) and maximized at d_{50} = 198.54 μm (148.53 mg/m^3).

CRediT authorship contribution statement

Hongliang Ding: Writing - original draft, Methodology, Data curation, Validation, Formal analysis, Investigation. **Ziqu Ouyang:** Supervision, Funding acquisition, Project administration. **Xiaoyu Zhang:** Data curation, Investigation. **Shujun Zhu:** Supervision, Investigation.

Declaration of Competing Interest

The authors declare that they have no known competing financial interests or personal relationships that could have appeared to influence the work reported in this paper.

Acknowledgments

Financial support of this work by National Key R&D Program of China (Project number 2017YFB0602001), the National Natural Science Foundation of China (No. 52006233) and Youth Innovation Promotion Association, CAS (2019148) are gratefully acknowledged.

References

[1] Wang J, Fan W, Li Yu, Xiao M, Wang K, Ren P. The effect of air staged combustion on NO_x emissions in dried lignite combustion. Energy 2012;37(1):725–36. https://doi.org/10.1016/j.energy.2011.10.007.
[2] Li Z, Liu G, Zhu Q, Chen Z, Ren F. Combustion and NO_x emission characteristics of a retrofitted down-fired 660Â MWe utility boiler at different loads. Appl Energy 2011;7:2400–6. https://doi.org/10.1016/j.apenergy.2011.01.048.
[3] Kuang M, Li Z, Zhang Y, Chen X, Jia J, Zhu Q. Asymmetric combustion characteristics and NO_x emissions of a down-fired 300 MWe utility boiler at different boiler loads. Energy 2012;1:580–90. https://doi.org/10.1016/j.energy.2011.10.046.
[4] Ouyang Z, Liu W, Zhu J, Liu J, Man C. Experimental research on combustion characteristics of coal gasification fly ash in a combustion chamber with a self-preheating burner. Fuel 2018;215:378–85. https://doi.org/10.1016/j.fuel.2017.11.047.
[5] Liu W, Ouyang Z, Cao X, Na Y. The influence of air-stage method on flameless combustion of coal gasification fly ash with coal self-preheating technology. Fuel 2019;235:1368–76. https://doi.org/10.1016/j.fuel.2018.08.127.
[6] Liu W, Ouyang Z, Na Y, Cao X, Liu D, Zhu S. Effects of the tertiary air injection port on semi-coke flameless combustion with coal self-preheating technology. Fuel 2020;271:117640. https://doi.org/10.1016/j.fuel.2020.117640.
[7] Ouyang Z, Ding H, Liu W, Cao X, Zhu S. Effect of the Primary Air Ratio on Combustion of the Fuel Preheated in a Self-preheating Burner. Combust Sci Technol 2020:1–18. https://doi.org/10.1080/00102202.2020.1808971.
[8] Fan JR, Liang XH, Chen LH, Cen KF. Modeling of NO_x emissions from a W-shaped boiler furnace under different operating conditions. Energy 1998;23(12):1051–5. https://doi.org/10.1016/S0360-5442(98)00059-0.
[9] Kuang M, Li Z. Review of gas/particle flow, coal combustion, and NO_x emission characteristics within down-fired boilers. Energy 2014;69:144–78. https://doi.org/10.1016/j.energy.2014.03.055.
[10] Wang Q, Chen Z, Che M, Zeng L, Li Z, Song M. Effect of different inner secondary-air vane angles on combustion characteristics of primary combustion zone for a down-fired 300-MWe utility boiler with overfire air. Appl Energy 2016;182:29–38. https://doi.org/10.1016/j.apenergy.2016.08.127.
[11] Chen Z, Wang Q, Wang B, Zeng L, Che M, Zhang X, et al. Anthracite combustion characteristics and NO_x formation of a 300 MWe down-fired boiler with swirl burners at different loads after the implementation of a new combustion system. Appl Energy 2017;189:133–41. https://doi.org/10.1016/j.apenergy.2016.12.063.
[12] Wang Q, Chen Z, Wang L, Zeng L, Li Z. Application of eccentric-swirl-secondary-air combustion technology for high-efficiency and low-NO_x performance on a large-scale down-fired boiler with swirl burners. Appl Energy 2018;223:358–68. https://doi.org/10.1016/j.apenergy.2018.04.064.
[13] Ren Q, Bao S. Combustion characteristics of ultrafine gasified semi-char in circulating fluidized bed. Can J Chem Eng 2016;94(9):1676–82. https://doi.org/10.1002/cjce:v94.910.1002/cjce:22562.
[14] Gong Z, Liu Z, Zhou T, Lu Q, Sun Y. Combustion and NO Emission of Shenmu Char in a 2 MW Circulating Fluidized Bed. Enegy & Fuels 2015;29(2):1219–26. https://doi.org/10.1021/ef502768w.
[15] Zhou T, Gong Z, Lu Q, Na Y, Sun Y. Experimental Study on Enhanced Control of NO_x Emission from Circulating Fluidized Bed Combustion. Energy Fuels 2015;29(6):3634–9. https://doi.org/10.1021/acs.energyfuels.5b00519.
[16] Zhou T, Lu Q, Cao Y, Wu G, Li S. Study on the combustion and NO_x emission characteristics of low rank coal in a circulating fluidized bed with post-combustion. Can J Chem Eng 2017;95(12):2333–40. https://doi.org/10.1002/cjce:22907.
[17] Oberlack M, Arlitt R, Peters N. On stochastic DamkAhler number variations in a homogeneous flow reactor. Combust Theor Model 2000;4:495–509. https://doi.org/10.1088/1364-7830/4/4/307.
[18] Kumar S, Paul PJ, Mukunda HS. Studies on a new high-intensity low-emission burner. Proc Combust Inst 2002;29(1):1131–7. https://doi.org/10.1016/S1540-7489(02)80143-2.
[19] Mancini M, Weber R, Bollettini U. Predicting NO_x emissions of a burner operated in flameless oxidation mode. Proc Combust Inst 2002;29(1):1155–63. https://doi.org/10.1016/S1540-7489(02)80146-8.
[20] Weidmann M, Verbaere G, Boutin D, Honore S, Grathwohl G, Goddard C. Detailed investigation of flameless oxidation of pulverized coal at pilot-scale (230 kWth). Appl Therm Eng 2015;74:96–101. https://doi.org/10.1016/j.applthermaleng.2014.01.039.
[21] Stadler H, Toporov D, Förster M, Kneer R. On the influence of the char gasification reactions on NO formation in flameless coal combustion. Combust Flame 2009;156(9):1755–63. https://doi.org/10.1016/j.combustflame.2009.06.006.
[22] Verssimo A, Rocha A, Costa M. Importance of the inlet air velocity on the establishment of flameless combustion in a laboratory combustor. Exp Therm Fluid Sci 2013;44:75–81. https://doi.org/10.1016/j.expthermflusci.2012.05.015.
[23] Katsuki M, Hasegawa T. The science and technology of combustion in highly preheated air. 27th Symposium (Intcrnation) on combustion, Pittsburgh: the Combustion Institute 1998; 27:3135-46.
[24] Lu Q, Zhu J, Niu T, Song G, Na Y. Pulverized coal combustion and NO_x emissions in high temperature air from circulating fluidized bed. Fuel Process Technol 2008;89(11):1186–92. https://doi.org/10.1016/j.fuproc.2008.05.008.
[25] Ouyang Z, Zhu J, Lu Q. Experimental study on preheating and combustion characteristics of pulverized anthracite coal. Fuel 2013;113:122–7. https://doi.org/10.1016/j.fuel.2013.05.063.
[26] Wang J, Zhu J-G, Lu Q-G. Experimental study on combustion characteristics and NO_x emissions of pulverized anthracite preheated by circulating fluidized bed. J Therm Sci 2011;20(4):355–61. https://doi.org/10.1007/s11630-011-0481-6.
[27] Yao Y, Zhu J, Lu Q, Zhou Z. Experimental study on preheated combustion of pulverized semi-coke. J Therm Sci 2015;24(4):370–7. https://doi.org/10.1007/s11630-015-0797-8.
[28] Zhu J, Ouyang Z, Lu Q. An Experimental Study on NO_x Emissions in Combustion of Pulverized Coal Preheated in a Circulating Fluidized Bed. Energy Fuels 2013;27(12):7724–9. https://doi.org/10.1021/ef402146w.
[29] Man C, Zhu J, Ouyang Z, Liu J, Lu Q. Experimental study on combustion characteristics of pulverized coal preheated in a circulating fluidized bed. Fuel Process Technol 2018;172:72–8. https://doi.org/10.1016/j.fuproc.2017.12.009.
[30] Ouyang Z, Liu W, Man C, Zhu J, Liu J. Experimental study on combustion, flame and NO_x emission of pulverized coal preheated by a preheating burner. Fuel Process Technol 2018;179:197–202. https://doi.org/10.1016/j.fuproc.2018.07.008.
[31] Yonmo S, Cheoreon M, Seongyong E, Gyungmin C, Duckjool K. Coal-particle size effects on NO reduction and burnout characteristics with air-staged combustion in a pulverized coal-fired furnace. Fuel 2016;182:558–67. https://doi.org/10.1016/j.fuel.2016.05.122.
[32] Casaca C, Costa M. NO_x control through reburning using biomass in a laboratory furnace: Effect of particle size. Proc Combust Inst 2009;32(2):2641–8. https://doi.org/10.1016/j.proci.2008.06.138.
[33] Abbas T, Costen P, Lockwood FC, Romo-Millares CA. The effect of particle size on NO formation in a large-scale pulverized coal-fired laboratory furnace: Measurements and modeling. Combust Flame 1993;93(3):316–26. https://doi.org/10.1016/0010-2180(93)90112-G.
[34] Li C, Dai Z, Sun Z, Li Z, Wang F. Development of a Comprehensive Model of Entrained Flow Coal Gasifier and Study of Effects of Particle Diameter on Gasification Results. J Chem Eng Chinese Universities 2013;27:597–603. https://doi.org/10.3969/j.issn.1003-9015.2013.04.009.
[35] Ouyang Z, Zhu J, Lu Q, Wang J, Hou H. Particle Characteristics of Anthracite Powder Preheated Quickly in Circulating Fluidized Bed. Proceedings of 2013 International Conference on Materials for Renewable Energy and Environment, BeiJing, China 2013: 6.
[36] Brunauer S, Emmett PH, Teller E. Adsorption of Gases in Multimolecular Layers. J Am Chem Soc 1938;60(2):309–19. https://doi.org/10.1021/ja01269a023.
[37] Webb P, Orr C. Analytical Methods in Fine Particle Technology. Norcross: Micromeritics Instrument Corp; 1997.
[38] Howard JB, Essenhigh RH. Mechanism of solid-partical combustion with simultaneous gas-phase volatiles combustion. Symposium on Combustion 1967;11(1):399–408. https://doi.org/10.1016/S0082-0784(67)80164-4.
[39] Chhiti Y, Salvador S, Commandre J-M, Broust Francois, Couhert C. Wood Bio-Oil Noncatalytic Gasification: Influence of Temperature, Dilution by an Alcohol and Ash Content. Energy Fuels 2011;25(1):345–51. https://doi.org/10.1021/ef101247m.
[40] Liu W, Ouyang Z, Cao X, Na Y. Experimental research on flameless combustion with coal preheating technology. Energy Fuels 2018;32(6):7132–41. https://doi.org/10.1021/acs.energyfuels.8b00719.
[41] Miller JA, Bowman CT. Mechanism and modeling of nitrogen chemistry in combustion. Process Energy Combustion Sci 1989;15(4):287–338. https://doi.org/10.1016/0360-1285(89)90017-8.
[42] Mitchell JW, Tarbell JM. A kinetic model of nitric oxideformation during pulverized coal combustion. AIChE J 1982;28(2):302–11. https://doi.org/10.1002/aic.690280220.
[43] Han X, Wei X, Schnell U, Hein KRG. Detailed modeling of hybrid reburn/SNCR processes for NO_x reduction in coal-fired furnaces. Combust Flame 2003;132(3):374–86. https://doi.org/10.1016/S0010-2180(02)00481-9.
[44] Courtemanche B, Levendis Y. A laboratory study on the NO, NO_2, SO_2, CO and CO_2 emissions from the combustion of pulverized coal, municipal waste plastics and tires. Fuel 1998;77:183–96. https://doi.org/10.1016/S0016-2361(97)00191-9.
[45] Glarborg P, Kristensen PG, Dam-Johansen K, Alzueta MU, Millera A, Bilbao R. Nitric oxide reduction by non-hydrocarbon fuels. Implications for reburning with gasification gases. Energy Fuels 2000;14(4):828–38.
[46] Okazaki K, Shishido H, Nishikawa T, Ohtake K. Separation of the basic factors affecting NO formation in pulverized coal combustion. Twentieth. Symp (Int) Combust 1985;20(1):1381–9. https://doi.org/10.1016/S0082-0784(85)80630-5.
[47] Kramlich JC, Seeker WR, Samuelsen GS. Observations of chemical effects accompanying pulverized coal thermal decomposition. Fuel 1988;67(9):1182–9. https://doi.org/10.1016/0016-2361(88)90034-8.
[48] Smoot LD, Hedman PO, Smith PJ. Pulverized-coal combustion research at Brigham Young University. Prog Energy Combust Sci 1984;10(4):359–441. https://doi.org/10.1016/0360-1285(84)90001-7.
[49] Schnell U, Kaess M, Brodbek H. Experimental and numerical investigation of NO_x formation and its basic interdependences on pulverized coal flame characteristics.

Combust Sci Technol 1993;93(1):91–109. https://doi.org/10.1080/00102209308935284.

[50] Barratt DJ, Roberts PT. The suitability of ultrafine coal as an industrial boiler fuel. Combust Flame 1989;77(1):51–68. https://doi.org/10.1016/0010-2180(89)90104-1.

[51] Kamal MM. Parametric study of combined premixed and non-premixed flame coal burner. Fuel 2008;87(8-9):1515–28. https://doi.org/10.1016/j.fuel.2007.09.002.